FirstPage

Pure Spin Current Injection in Hydrogenated Graphene Structures

Reinaldo Zapata-Peña[1], Bernardo S. Mendoza[1], Anatoli I. Shkrebtii[2]

[1]*Centro de Investigaciones en Óptica, León, Guanajuato 37150, México and*

[2]*University of Ontario, Institute of Technology, Oshawa, ON, L1H 7L7, Canada*

(Dated: April 26, 2017)

Lorem ipsum dolor sit amet, consectetuer adipiscing elit. Etiam lobortis facilisis sem. Nullam nec mi et neque pharetra sollicitudin. Praesent imperdiet mi nec ante. Donec ullamcorper, felis non sodales commodo, lectus velit ultrices augue, a dignissim nibh lectus placerat pede. Vivamus nunc nunc, molestie ut, ultricies vel, semper in, velit. Ut porttitor. Praesent in sapien. Lorem ipsum dolor sit amet, consectetuer adipiscing elit. Duis fringilla tristique neque. Sed interdum libero ut metus. Pellentesque placerat. Nam rutrum augue a leo. Morbi sed elit sit amet ante lobortis sollicitudin. Praesent blandit blandit mauris. Praesent lectus tellus, aliquet aliquam, luctus a, egestas a, turpis. Mauris lacinia lorem sit amet ipsum. Nunc quis urna dictum turpis accumsan semper.

I. INTRODUCTION

Lorem ipsum dolor sit amet, consectetuer adipiscing elit. Etiam lobortis facilisis sem. Nullam nec mi et neque pharetra sollicitudin. Praesent imperdiet mi nec ante. Donec ullamcorper, felis non sodales commodo, lectus velit ultrices augue, a dignissim nibh lectus placerat pede. Vivamus nunc nunc, molestie ut, ultricies vel, semper in, velit. Ut porttitor. Praesent in sapien. Lorem ipsum dolor sit amet, consectetuer adipiscing elit. Duis fringilla tristique neque. Sed interdum libero ut metus. Pellentesque placerat. Nam rutrum augue a leo. Morbi sed elit sit amet ante lobortis sollicitudin. Praesent blandit blandit mauris. Praesent lectus tellus, aliquet aliquam, luctus a, egestas a, turpis. Mauris lacinia lorem sit amet ipsum. Nunc quis urna dictum turpis accumsan semper. Lorem ipsum dolor sit amet, consectetuer adipiscing elit. Etiam lobortis facilisis sem. Nullam nec mi et neque pharetra sollicitudin. Praesent imperdiet mi nec ante. Donec ullamcorper, felis non sodales commodo, lectus velit ultrices augue, a dignissim nibh lectus placerat pede. Vivamus nunc nunc, molestie ut, ultricies vel, semper in, velit. Ut porttitor. Praesent in sapien. Lorem ipsum dolor sit amet, consectetuer adipiscing elit. Duis fringilla tristique neque. Sed interdum libero ut metus. Pellentesque placerat. Nam rutrum augue a leo.

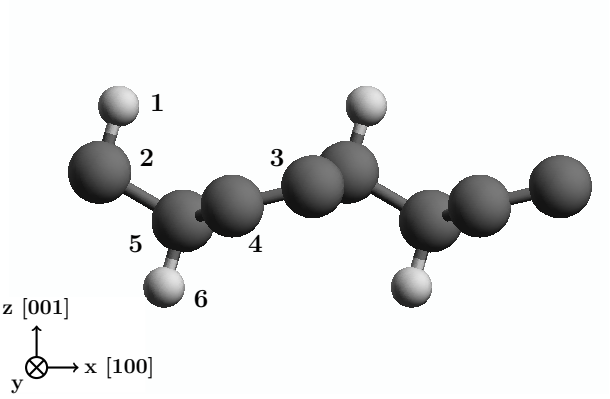

(a) *xz* plane view fig:alt-struc-xz

(b) *xy* plane view fig:alt-struc-xy

FIG. 1. Alt structure fig:alt-struc

Morbi sed elit sit amet ante lobortis sollicitudin. Praesent blandit blandit mauris. Praesent lec-

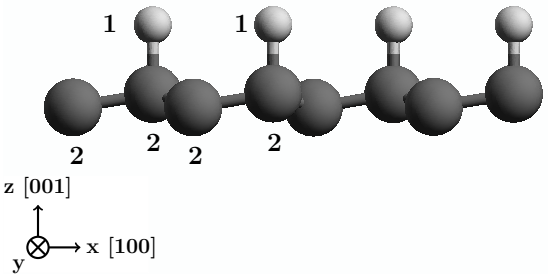

(a) xz plane view fig:up-struc-xz

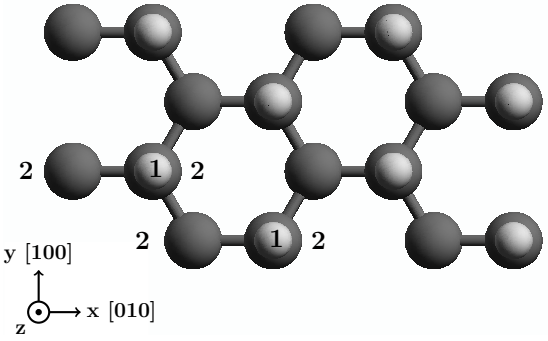

(b) xy plane view fig:up-struc-xy

FIG. 2. Up structure fig:up-struc

tus tellus, aliquet aliquam, luctus a, egestas a, turpis. Mauris lacinia lorem sit amet ipsum. Nunc quis urna dictum turpis accumsan semper. Lorem ipsum dolor sit amet, consectetuer adipiscing elit. Etiam lobortis facilisis sem. Nullam nec mi et neque pharetra sollicitudin. Praesent imperdiet mi nec ante. Donec ullamcorper, felis non sodales commodo, lectus velit ultrices augue, a dignissim nibh lectus placerat pede. Vivamus nunc nunc, molestie ut, ultricies vel, semper in, velit. Ut porttitor. Praesent in sapien. Lorem ipsum dolor sit amet, consectetuer adipiscing elit. Duis fringilla tristique neque. Sed interdum libero ut metus. Pellentesque placerat. Nam rutrum augue a leo. Morbi sed elit sit amet ante lobortis sollicitudin. Praesent blandit blandit mauris. Praesent lectus tellus, aliquet aliquam, luctus a, egestas a, turpis. Mauris lacinia lorem sit amet ipsum. Nunc quis urna dictum turpis accumsan semper.

Lorem ipsum dolor sit amet, consectetuer adipiscing elit. Etiam lobortis facilisis sem. Nullam nec mi et neque pharetra sollicitudin. Praesent imperdiet mi nec ante. Donec ullamcorper, felis non sodales commodo, lectus velit ultrices augue, a dignissim nibh lectus placerat pede. Vivamus nunc nunc, molestie ut, ultricies vel, semper in, velit. Ut porttitor. Praesent in sapien. Lorem ipsum dolor sit amet, consectetuer adipiscing elit. Duis fringilla tristique neque. Sed interdum libero ut metus. Pellentesque placerat. Nam rutrum augue a leo. Morbi sed elit sit amet ante lobortis sollicitudin. Praesent blandit blandit mauris. Praesent lectus tellus, aliquet aliquam, luctus a, egestas a, turpis. Mauris lacinia lorem sit amet ipsum. Nunc quis urna dictum turpis accumsan semper.

II. THEORY

sec:theory

The equation for $\mathcal{V}^{\mathrm{ab}}$ for normal incidence in the xy plane with a polarization angle α is given by

$$\begin{aligned}\mathcal{V}^{\mathrm{ab}}(\omega) &= \frac{2}{\hbar}\frac{\mu^{\mathrm{abxx}}(\omega)E^2(\omega)\cos^2(\alpha)+\mu^{\mathrm{abyy}}(\omega)E^2(\omega)\sin^2(\alpha)+2\mu^{\mathrm{abxy}}(\omega)E^2(\omega)\cos(\alpha)\sin(\alpha)}{\xi^{\mathrm{xx}}(\omega)E^2(\omega)\cos^2(\alpha)+\xi^{\mathrm{yy}}(\omega)E^2(\omega)\sin^2(\alpha)},\\ &= \frac{2}{\hbar}\frac{\mu^{\mathrm{abxx}}(\omega)\cos^2(\alpha)+\mu^{\mathrm{abyy}}(\omega)\sin^2(\alpha)+\mu^{\mathrm{abxy}}(\omega)\sin(2\alpha)}{\xi^{\mathrm{xx}}(\omega)\cos^2(\alpha)+\xi^{\mathrm{yy}}(\omega)\sin^2(\alpha)}. \qquad (1)\end{aligned}$$

eq:vab

For an angle $\alpha = \frac{\pi}{4}$ this expression can be reduced to

$$\mathcal{V}^{\mathrm{ab}}(\omega) = \frac{2}{\hbar}\frac{\mu^{\mathrm{abxx}}(\omega)+\mu^{\mathrm{abyy}}(\omega)+2\mu^{\mathrm{abxy}}(\omega)}{\xi^{\mathrm{xx}}(\omega)+\xi^{\mathrm{yy}}(\omega)}. \qquad (2)$$

eq:vab-90deg

A. Fixing velocity.

sec:theory-fixvel

Considering that we have 2D structures we fixed the velocity in the xy plane along x and y directions and we define $|\mathcal{V}^{\rm a}|$ as

$$|\mathcal{V}^{\rm a}| = \sqrt{(\mathcal{V}^{\rm ax})^2 + (\mathcal{V}^{\rm ay})^2 + (\mathcal{V}^{\rm az})^2}, \quad (3)$$

eq:va-mag

and the corresponding polar and azimuthal angles θ and φ as

$$\theta = \cos^{-1}\left(\frac{\mathcal{V}^{\rm az}}{|\mathcal{V}^{\rm a}|}\right), \qquad 0 \leq \theta \leq \pi, \quad (4)$$

eq:polar-ang

$$\varphi = \tan^{-1}\left(\frac{\mathcal{V}^{\rm ay}}{\mathcal{V}^{\rm ax}}\right), \qquad 0 \leq \varphi \leq 2\pi. \quad (5)$$

eq:azimuthal-ang

B. Fixing spin

sec:theory-fixspin

In a similar way we can fix in the xy plane the spin direction along the x, y, and z directions and then define the magnitude of the spin velocity $|\mathcal{V}_{\sigma^{\rm b}}|$ in a fixed angle γ_b

$$|\mathcal{V}_{\sigma^{\rm b}}| = \sqrt{(\mathcal{V}^{\rm ax})^2 + (\mathcal{V}^{\rm ay})^2}, \quad (6)$$

$$\gamma_{\rm b} = \tan^{-1}\left(\frac{\mathcal{V}^{\rm ay}}{\mathcal{V}^{\rm ax}}\right), \quad (7)$$

where the angle is measured in the counterclockwise direction from the positive x axis.

III. RESULTS

sec:results

We preset the results for $\mathcal{V}^{\rm ab}$ for the $C_{16}H_8$-alt and $C_{16}H_8$-up structures being both noncentrosymmetric semi-infinite carbon systems with 50% hydrogenation in different arrangements. The *alt* system has alternating hydrogen atoms on the upper and bottom sides of the carbon sheet, while the *up* system has H only on the upper side. We take the hexagonal carbon lattice to be on the xy plane for both structures, and the carbon-hydrogen bonds on the perpendicular xz plane, as depicted in Figs. 1 and 2.

Using the ABINIT code[1] we calculated the self- consistent ground state and the Kohn-Sham states using density functional theory in the local density approximation (DFT-LDA) with a planewave basis. We used Hartwigsen-Goedecker-Hutter (HGH) relativistic separable dual-space Gaussian pseudopotentials[2] including the spin-orbit interaction for calculating $\mathcal{V}^{\rm a}(\omega)$.

Layer No.	Atom type	Position [Å] x	y	z
1	H	-0.61516	-1.42140	1.47237
2	C	-0.61516	-1.73300	0.39631
3	C	0.61516	1.73300	0.15807
4	C	0.61516	0.42201	-0.15814
5	C	-0.61516	-0.37396	-0.39632
6	H	-0.61516	-0.68566	-1.47237

TABLE I. Unit cell of *alt* structure. Layer division, atom types and positions for the *alt* structure. The structure unit cell was divided in six layers corresponding each one to atoms in different z positions. The corresponding layer atom position is depicted in Fig. 1 with the corresponding number of layer.

tab:alt-unitcell

The convergence parameters for the calculations of our results corresponding to the *alt* and *up* structures are cutoff energies of 65 Ha and 40 Ha, respectively. The energy eigenvalues and matrix elements were calculated using 14452 **k** points and 8452 **k** points in the irreducible Brillouin zone (IBZ) and present LDA energy band gaps of 0.72 eV and 0.088 eV, respectively for the *alt* and *up* structures. As mentioned in[3], using DFT the LDA is only one method of many other that can be used to calculate the electronic structure of materials. Also it is known that all methods predict a different band gap than the obtained in the experiment. A correction for the band gap energy value can be calculated by other *ab-initio* methods such as the GW approximation[4] being this outside the scope of this paper.

The structures presented here where divided into layers to analyze the he layer-by-layer contribution for $\mathcal{V}^{\rm ab}$ response. The *alt* structure was divided in six layers corresponding the first one to the top hydrogen atoms, from the second to the forth to carbon atoms in different z positions, and the sixth and last one to the bottom hydrogen atoms. The *up* structure was divided into two layers, the first one comprised by the top hydrogen atoms and the second by the carbon atoms. The layer divisions and atom positions

Layer No.	Atom type	Position [Å] x	y	z
1	H	-0.61516	-1.77416	0.73196
1	H	0.61518	0.35514	0.73175
2	C	-0.61516	-1.77264	-0.49138
2	C	-0.61516	-0.35600	-0.72316
2	C	0.61516	0.35763	-0.49087

TABLE II. Unit cell of *up* structure. Layer division, atom types and positions for the *up* structure. The structure unit cell was divided in two layers corresponding to hydrogen and carbon atoms.The corresponding layer atom position is depicted in Fig. 2 with the corresponding number of layer.

tab:up-unitcell

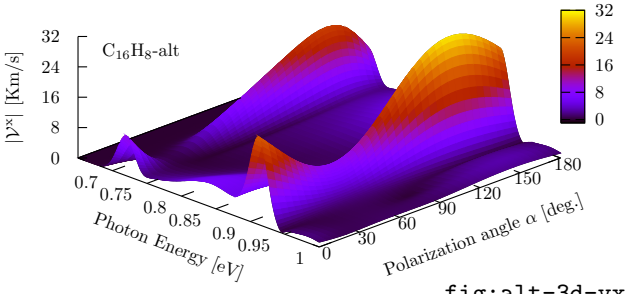

(a) $|\mathcal{V}^{\mathrm{x}}|$ for *alt* structure

fig:alt-3d-vx

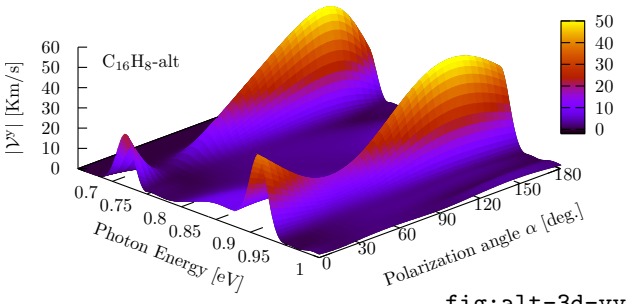

(b) $|\mathcal{V}^{\mathrm{x}}|$ for *alt* structure

fig:alt-3d-vy

FIG. 3. $|\mathcal{V}^{\mathrm{x}}|$ response for $C_{16}H_8$-alt structure. The maximum response zone is localized for an energy range from 0.90 eV to 0.93 eV and for a polarization angle of the incoming beam from 120° to 150°.

fig:alt-3d

for the unit cells are shown in Tables I and II.

A. Fixing velocity

sec:res-fixvel

For the *alt* structure we analyzed the energy range from 0.6 eV to 1.0 eV where we found the most intense response for $|\mathcal{V}^{\mathrm{x}}|$ and $|\mathcal{V}^{\mathrm{a}}|$. In Fig. 3 we present the $|\mathcal{V}^{\mathrm{a}}|$ spectra resulting from evaluate Eq. (3) using different polarization angles α in Eq. (1) for the $C_{16}H_8$-alt structure. We can see that the onset of the response is when the energy of the incoming light is the same of the gap energy. From this picture we can see that for the zone between the energy range of 0.90 eV-0.93 eV and polarization angles between 120° and 150° is

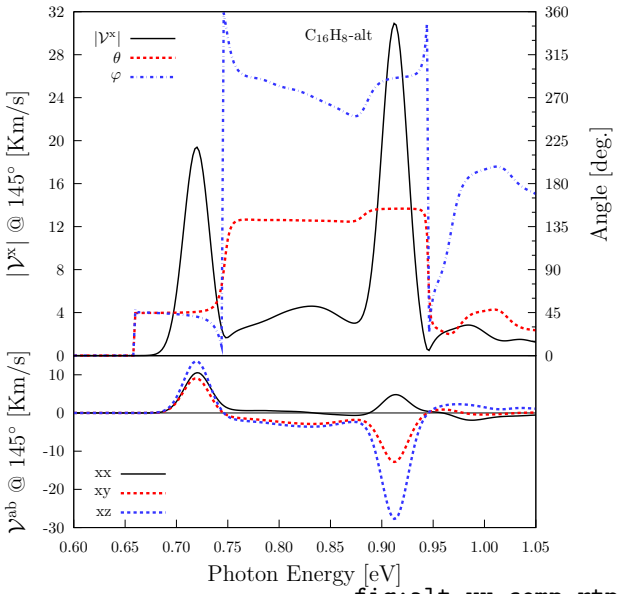

(a) $|\mathcal{V}^{\mathrm{x}}|$

fig:alt-vx-comp-rtp

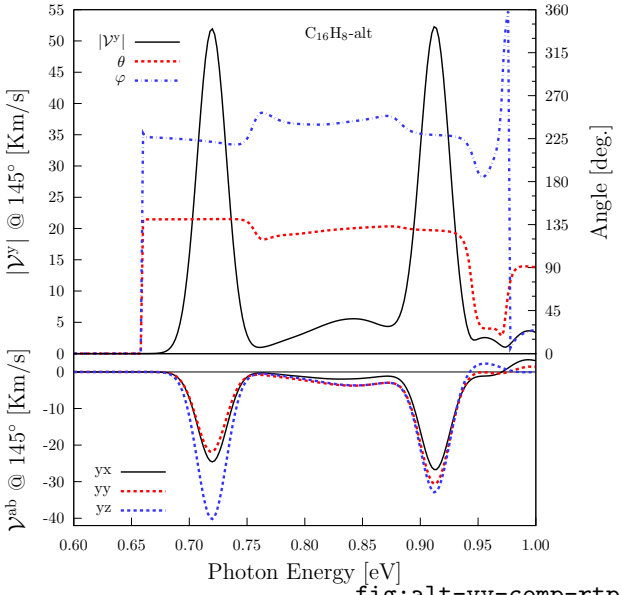

(b) $|\mathcal{V}^{\mathrm{y}}|$

fig:alt-vy-comp-rtp

FIG. 4. Most intense responses of $|\mathcal{V}^{\mathrm{x}}|$ and $|\mathcal{V}^{\mathrm{y}}|$ and the corresponding three components for the *alt* structure. Both maxima where obtained for a polarization angle $\alpha = 145°$.

fig:alt-vab-comp-rtp

the zone of the absolute maximum response for both, $|\mathcal{V}^{x}|$ and $|\mathcal{V}^{y}|$. Also there is another zone of interest for energies from 0.70 eV to 0.74 eV and same polarization angles range where a local maximum is obtained. From Figs. 3(a) and 3(b) we have that $|\mathcal{V}^{x}|$ reaches values of 30 Km/s and 20 Km/s, respectively. We also found that the absolute maximum of the response is obtained when the polarization angle is $\alpha = 145°$. In the top frames of Figs. 4(a) and 4(b) we present the results for $|\mathcal{V}^{x}|$ and $|\mathcal{V}^{y}|$ fixing the polarization angle to 145° for the *alt* structure vs the photon energy and the corresponding polar φ and azimuthal θ angles. Also in the bottom frames of Figs. 4(a) and 4(b) we present the decomposition of $|\mathcal{V}^{x}|$ and $|\mathcal{V}^{y}|$ in the corresponding $\mathcal{V}^{xx}$, $\mathcal{V}^{xy}$, $\mathcal{V}^{xz}$ and $\mathcal{V}^{yx}, \mathcal{V}^{yy}$ $\mathcal{V}^{yz}$ components for the fixed polarization angle. Making the analysis for the components and angles for $|\mathcal{V}^{x}|$ depicted in Fig. 4(a) we can see that for the energy range from 0.70 eV to 0.74 eV all the xx, xy, and xz components contribute with almost the same intensity giving a total spin- velocity of 19.3 Km/s and spin polar and azimuthal angles $\varphi = 45.8°$ and $\theta = 40.7°$. In the other hand, for the energy range from 0.88 eV to 0.95 eV there is a major contribution coming from the $\mathcal{V}^{xz}$ component resulting in a spin-velocity magnitude of 30.9 Km/s being this magnitude the most intense for $|\mathcal{V}^{x}|$. In this case the polar angle is $\varphi = 153.8°$ and the spin angle over the xy plane have is $\theta = 290.4°$. Also we notice that for the range of 0.70-0.74 eV all the contributions are positive while for the range of 0.88-0.95 eV the xx component remains positive but the components xy and xz change in direction. This is due to a change in the spin polarization. Making now the analysis for $|\mathcal{V}^{y}|$ depicted in Fig. 4(b) we have that for the energy range from 0.70 eV to 0.74 eV the yz component have a more intense response than yx and yy components and they give a total spin-velocity of 51.9 Km/s and result in polar angle $\varphi = 140.7°$ and spin azimuthal angle of $\theta = 221.5°$. For the energy range from 0.88 eV to 0.95 eV all three components have similar intensities resulting in a spin-velocity magnitude of $|\mathcal{V}^{y}| = 52.3$ Km/s being this response 1.7 times mores intense than the most intense response of $|\mathcal{V}^{x}|$. The corresponding polar and azimuthal angles for $|\mathcal{V}^{y}|$ in this energy range are $\theta = 129.0°$ and $\varphi = 228.9°$. Now we have that the three components of $|\mathcal{V}^{y}|$ are negative for the energy range from 0.60 eV to 1.0 eV keeping the same spin polarization for all this range.

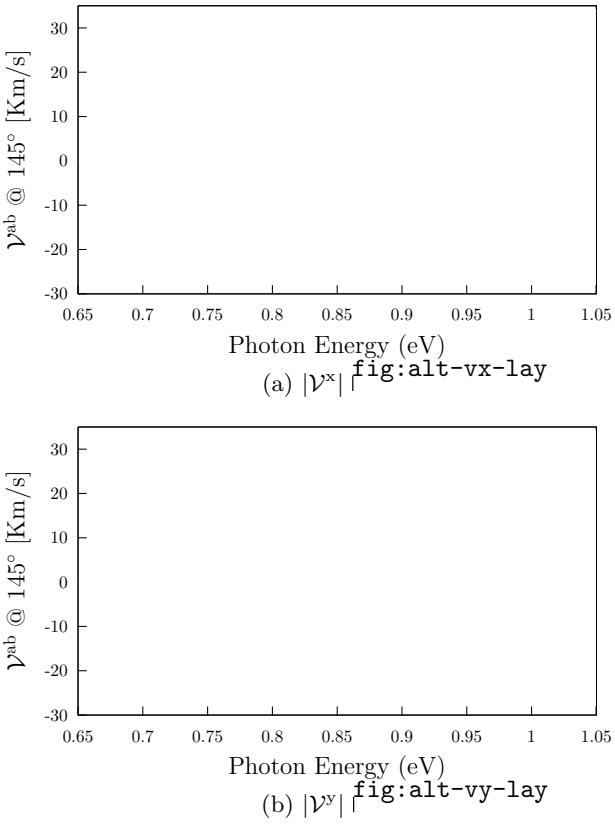

FIG. 5. Layer-by-layer contribution of $|\mathcal{V}^{x}|$ and $|\mathcal{V}^{y}|$ for a polarization angle $\alpha = 145°$ for the *alt* structure.
fig:alt-vab-lay

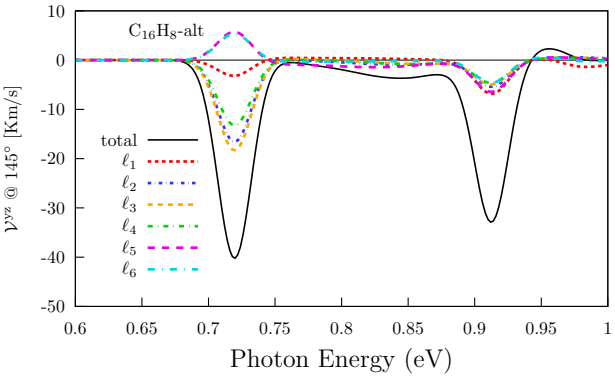

FIG. 6. Layer-by-layer contribution of $\mathcal{V}^{yz}$ for the *alt* structure.
fig:alt-vyz-lay

In Fig. 5 we show the layer-by-layer contribution of $|\mathcal{V}^{ab}|$ for the *alt* structure. The cor-

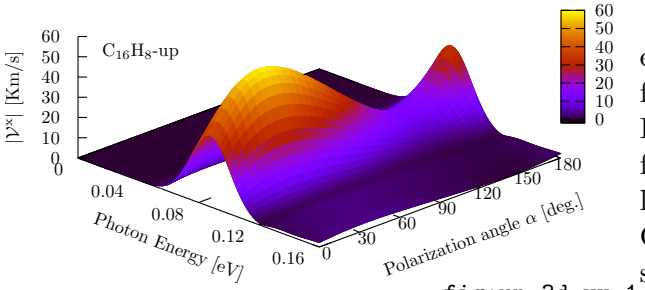

(a) $|\mathcal{V}^{x}|$ for *up* structure fig:up-3d-vx-1

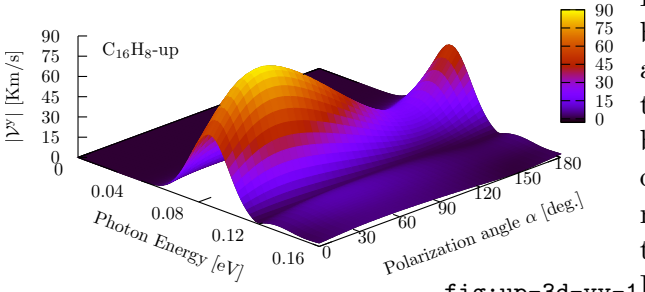

(b) $|\mathcal{V}^{x}|$ for *up* structure fig:up-3d-vy-1

FIG. 7. $|\mathcal{V}^{x}|$ response for $C_{16}H_8$-up structure. The maximum response zone is localized for an energy range from 0.04 eV to 0.12 eV and for a polarization angle of the incoming beam from 25° to 50°. fig:up-3d-1

responding layer division and atom types and positions are presented in Table I and depicted in Fig. 1. In the layer- by-layer contribution for $|\mathcal{V}^{x}|$ (Fig. 5(a)) we have that ... Also, for the layer-by-layer contribution for $|\mathcal{V}^{y}|$ (Fig. 5(b)) we have that ... From the bottom panels of Fig. 4 we can see that for the *alt* structure the most intense component of $|\mathcal{V}^{x}|$ and $|\mathcal{V}^{y}|$ corresponds to $\mathcal{V}^{yz}$ which has a value of -40.21374498 Km/s for an energy incident beam of 0.72 eV. This component and the corresponding layer by layer contribution is depicted in Fig. 6. From this figure we have that for the energy range from 0.70 eV to 0.74 eV the fifth and sixth layers corresponding to the bottom carbon and hydrogen numbered with 5 and 6 in Fig. 1 have contributions in opposite direction than the other 4 layers resulting in a total response $\mathcal{V}^{yz} = -40.2$ Km/s for an incoming beam energy of 0.72 eV. In the other hand, for the energy range from 0.88 eV to 0.95 eV the response for the all six layers the responses are in the same direction resulting in a total response $\mathcal{V}^{yz} = -32.89$ Km/s for an incoming beam with energy of 0.912 eV.

For the *up* structure we first analyzed the energy range from 0.00 eV to 0.16 eV where we found the most intense response for $\mathcal{V}^{x}$ and $|\mathcal{V}^{y}|$. In Fig. 7 we present the $\mathcal{V}^{a}$ spectra resulting from evaluate again Eq. (3) using different polarization angles α in Eq. (1) but now for the $C_{16}H_8$-up structure. We can see that the onset of the response is when the energy of the incoming light is the same of the gap energy. From this picture we can see that for the zone between the energy range of 0.084 eV-0.093 eV and polarization angles between 30° and 45° is the zone of the absolute maximum response for both, $|\mathcal{V}^{x}|$ and $|\mathcal{V}^{y}|$. Also there is another zone of interest, depicted in Fig. 8, where a local maximum is obtained for energies from 0.95 eV to 0.99 eV and same polarization angles. From Figs. 8(a) ad 8(b) we have that $|\mathcal{V}^{x}|$ and $|\mathcal{V}^{y}|$ reach values of 10 Km/s and 50 Km/s, respectively. We found that the absolute maximum of the response is obtained when the polarization angle is $\alpha = 40°$. In the top frames of Figs. 9 and 10 we present the results for $|\mathcal{V}^{x}|$ and $|\mathcal{V}^{y}|$ fixing the polarization angle to 40° for the *up*

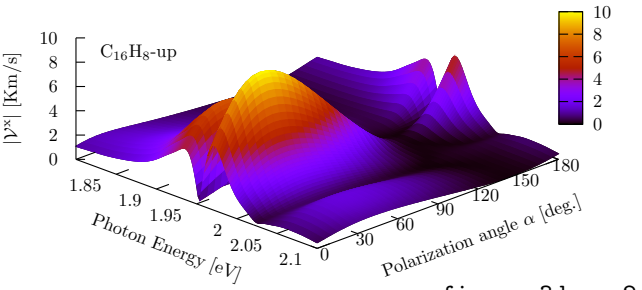

(a) $|\mathcal{V}^{x}|$ for *up* structure fig:up-3d-vx-2

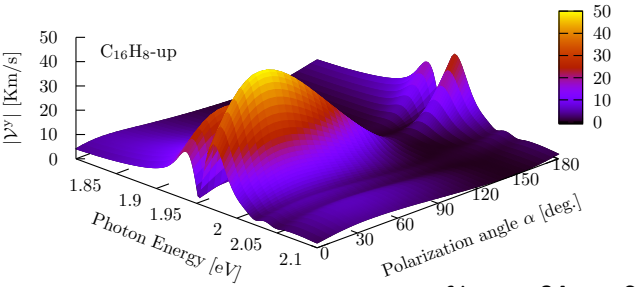

(b) $|\mathcal{V}^{x}|$ for *up* structure fig:up-3d-vy-2

FIG. 8. $|\mathcal{V}^{x}|$ response for $C_{16}H_8$-up structure. The local maximum response zone is localized for an energy range from 1.95 eV to 2.00 eV and for a polarization angle of the incoming beam from 25° to 50°. fig:up-3d-2

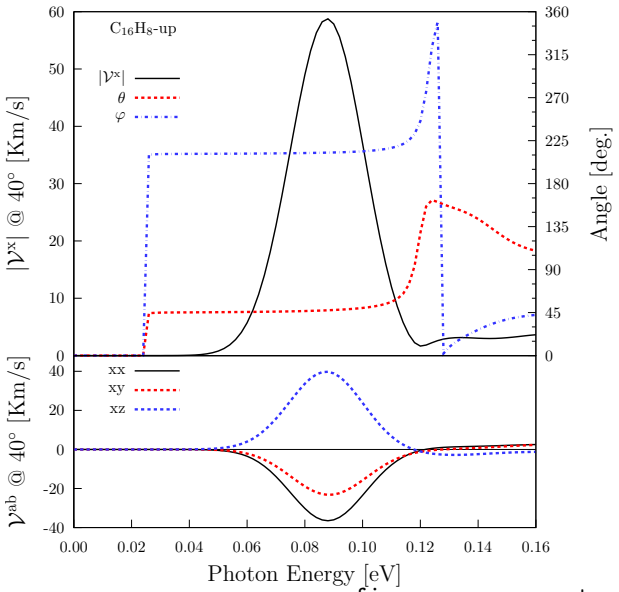

(a) $|\mathcal{V}^{\mathrm{x}}|$ fig:up-vx-comp-rtp-1

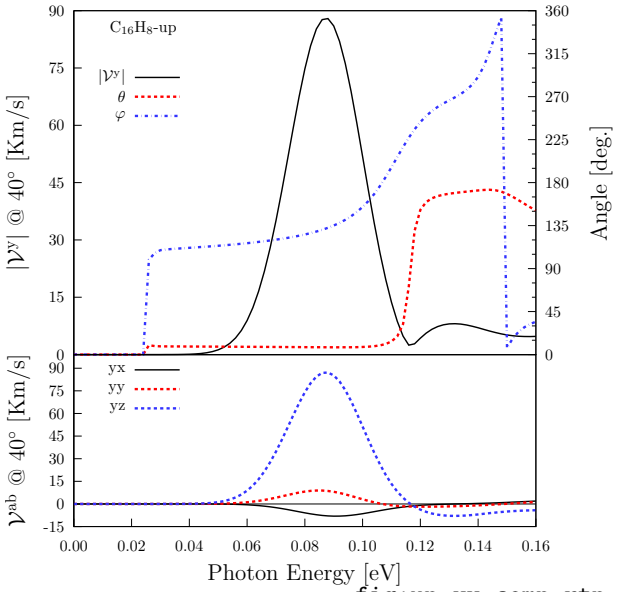

(b) $|\mathcal{V}^{\mathrm{y}}|$ fig:up-vy-comp-rtp-1

FIG. 9. Most intense responses of $|\mathcal{V}^{\mathrm{x}}|$ and $|\mathcal{V}^{\mathrm{y}}|$ and the corresponding three components for the *up* structure. Both maxima where obtained for a polarization angle $\alpha = 40°$. fig:up-vab-comp-rtp-1

structure vs the photon energy and the corresponding polar φ and azimuthal θ angles for the energy range from 0.0 eV to 0.16 eV and from

[1] X. Gonze, B. Amadon, P.-M. Anglade, J.-M. Beuken, F. Bottin, P. Boulanger, F. Bruneval, D. Caliste, R. Caracas, M. Côté, T. Deutsch, L. Genovese, P. Ghosez, M. Giantomassi, S. Goedecker, D. Hamann, P. Hermet, F. Jollet, G. Jomard, S. Leroux, M. Mancini, S. Mazevet, M. Oliveira, G. Onida, Y. Pouillon, T. Rangel, G.-M. Rignanese, D. Sangalli, R. Shaltaf, M. Torrent, M. Verstraete, G. Zerah, and J. Zwanziger, Comput. Phys. Commun. **180**, 2582 (2009).

[2] C. Hartwigsen, S. Goedecker, and J. Hutter, Phys. Rev. B **58**, 3641 (1998).

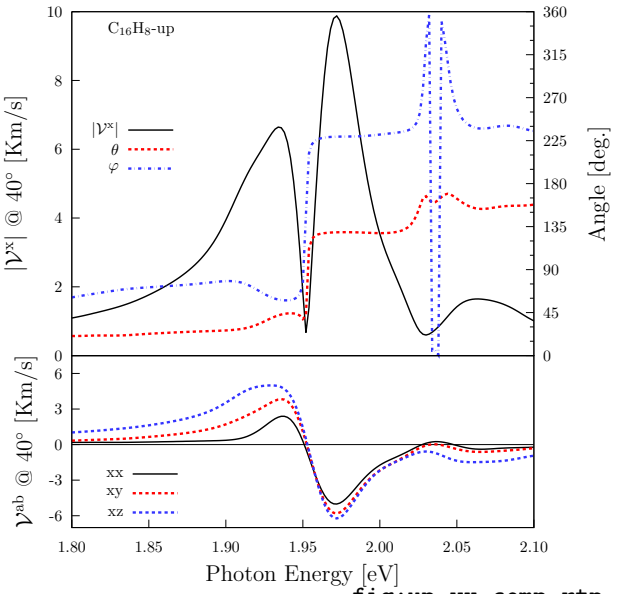

(a) $|\mathcal{V}^{\mathrm{x}}|$ fig:up-vx-comp-rtp-2

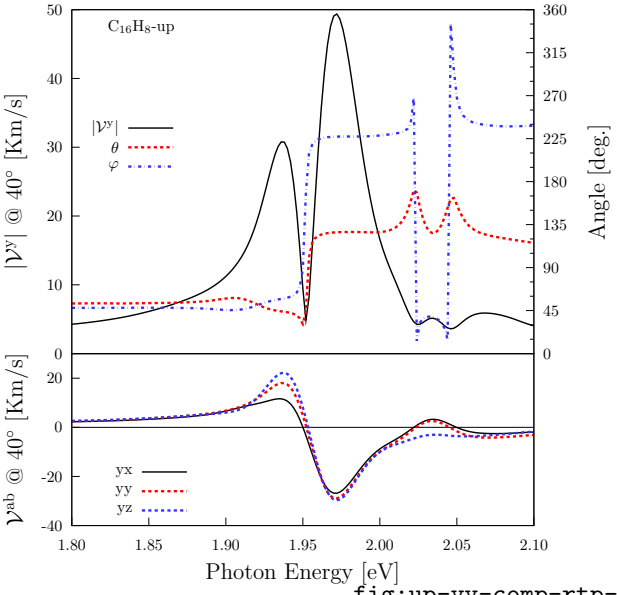

(b) $|\mathcal{V}^{\mathrm{y}}|$ fig:up-vy-comp-rtp-2

FIG. 10. Intense responses of $|\mathcal{V}^{\mathrm{x}}|$ and $|\mathcal{V}^{\mathrm{y}}|$ and the corresponding three components for the *up* structure. Both maxima where obtained for a polarization angle $\alpha = 40°$. fig:up-vab-comp-rtp-2

3 R. Zapata-Peña, S. M. Anderson, B. S. Mendoza, and A. I. Shkrebtii, physica status solidi (b) **253**, 226 (2016).

4 G. Onida, L. Reining, and A. Rubio, Rev. Mod. Phys. **74**, 601 (2002). LastBibItem